Atmospheric Research 248 (2021) 105186

Contents lists available at ScienceDirect

Atmospheric Research

journal homepage: www.elsevier.com/locate/atmosres

Mesocyclonic and non-mesocyclonic convective storms in Germany: Storm characteristics and life-cycle

Kathrin Wapler

Deutscher Wetterdienst, Offenbach, Germany

ARTICLE INFO

Keywords:
Thunderstorm
Lightning
Supercell
Mesocyclone
Life-cycle
Nowcasting

ABSTRACT

A multi-year analysis of mesocyclonic (approximately 4300) and non-mesocyclonic convective storms (more than 100,000) is presented. A comprehensive data set is generated which includes measurements from a lightning location system, a precipitation radar network, as well as information from automated cell detection algorithms based on radar reflectivity and radial winds. Storms' rotation, reflectivity, lightning and motion characteristics are analysed for storms with different lifetimes. Furthermore, the temporal evolution of the storms' attributes is analysed in order to study the convective life-cycle. For this purpose, the storms are grouped according to their lifetime. The temporal evolution of storm attributes varies from one storm to the other, however, typical storm developments are revealed. The average temporal evolution of the storm size is symmetric, the maximum is reached at the half of the lifetime. In contrast, the maximum lightning rate is reached later. Comparing the attributes of non-mesocyclonic and mesocyclonic storms, varies differences are identified. Mesocyclonic storms are shown to be typically longer-living (the median is approximately 30 min longer), larger, faster moving (on average approximately 15 km/h faster) and electrically more active compared to non-mesocyclonic storms. These characteristics are more pronounced for stronger mesocyclonic storms.

1. Introduction

Convective storms (including associated phenomena such as lightning, hail, damaging wind, heavy precipitation, tornadoes) pose a significant threat to life, property and economy. They may cause high damages and economic losses. A good knowledge of typical characteristics of convective storms might help in developing successful nowcasting systems to support severe weather warnings which are relevant for many sectors, including transportation, hydrology, general public and civil protection. Wapler et al. (2018) and Schmid et al. (2019) provide an overview of the current status of nowcasting systems applied at several European National Meteorological Services. They summarise that nowcasting approaches will benefit from a multiple data approach and the provision of life-cycle information (e.g. strengthening and weakening of convective weather events).

Studies from different geographical regions revealed that most of the storms producing significant hail are supercells. E.g. this was shown for parts of the Midwestern United States and Central Plains (Duda and Gallus, 2010), for Finland (Tuovinen et al., 2015) and Germany (Wapler, 2017).

Furthermore, analyses by Blair et al. (2017) comparing the storm maximum hail size with convective mode revealed much larger hail diameter in supercells compared to hail from non-supercellular storms. Blair et al. (2017) suggest to employ an approach for hail size forecasting using storm-mode in conjunction with other hail detection techniques (e.g. based on radar observations) to better anticipate and forecast hail sizes. Thus, it is useful to distinguish between cells containing rotation (mesocyclonic storms) and those that do not (non-mesocyclonic storms).

Deep convective storms in Germany and some adjacent regions are studied, focussing on their radar reflectivity, rotation and lightning characteristics. Large data sets are essential to cover a wide spectrum of possible convective developments. A 5-year time period is available to compare non-mesocyclonic and mesocyclonic storms. An 11-year time period is the basis for those parts of the analyses not distinguishing between non-mesocyclonic and mesocyclonic storms. Recent studies revealed the weather patterns that are most often inducing thunderstorms (Wapler and James, 2015) and mesocyclonic storms (Wapler et al., 2016) in the analysed domain.

The data used in the present study is introduced in Section 2. Section 3 shows the temporal and spatial occurrence of storms in the analysis domain. The storms attributes are described in Section 4, these include the storms motion, the storm intensity and the storm lifetime respectively. The life-cycle is discussed in Section 5. Finally, Section 6 provides a summary and some concluding remarks.

2. Data

The study domain covers Germany and some adjacent regions. The analysis uses a multi data approach, including convective cell

https://doi.org/10.1016/j.atmosres.2020.105186
Received 30 August 2019; Received in revised form 30 July 2020; Accepted 6 August 2020
Available online 15 August 2020

detections based on radar reflectivity measurements, mesocyclone detections using radar radial wind data and total lightning (cloud-to-ground and intra-cloud) measurements from a lightning location system. The individual data sets are described in the following.

2.1. Convective cell detection

Within the German C-band weather radar network (Mammen et al., 2010) a 5 min repetitive terrain-following near-surface scan is performed at each of the 17 operational stations. The range and azimuth resolutions are 1 km and 1°, respectively. The height of the measurements is close to the surface at the radar site. Depending on the topography as well as the atmospheric conditions and its influence on the radiation propagation, the height of the measurements rises with distance from the radar. These terrain-following radar sweeps from the individual radar sites are combined to a reflectivity composite covering Germany and some adjacent regions with a resolution of 1 km^2. (Additionally, a volume scan consisting of 10 sweeps with elevations from 0.5° up to 25° is performed with a 5 min (15 min before November 2012) interval. However, reflectivity measurements of the volume scans are so far not used for operational automatic cell detection and tracking. A 3D cell detection algorithm is currently under development (Werner, 2017).)

For the present study data from the cell detection and tracking algorithm KONRAD (*KONvektionsentwicklung in RADarprodukten*, convection evolution in radar products, Lang, 2001) is used. It runs operationally every 5 min using the 2D reflectivity composite. KONRAD defines a convective cell as a continuous area of radar reflectivity of 46 dBZ or more with a size of at least 15 km^2. Using consecutive radar images cells are also followed over time providing cell tracks.

In the case of cell splitting, two situations are possible: KONRAD follows one of the cells with the same ID and allocates a new ID to the other cell, or allocates a new ID to both of the cells after cell splitting. This could lead to an unrealistically short cell track. Thus, the real lifetime of the convective cells might be longer. In the case of cell merging, the following two situations may occur: the merged cell gets the ID of one of the contributing cells or KONRAD allocates a new ID. Cell splits and merges are a challenge for any cell detection and tracking algorithm. One reason is the lack of a unique definition of a convective cell. To avoid effects that may arise from inappropriate ID attribution, only cells with Category 0 (see below) at the time of its first detection are considered in the life-cycle analysis.

Cell attributes that are provided by KONRAD include the following: cell location (coordinates of the cell centre), movement speed and direction, cell size (area with equal or more than 46 dBZ), and cell core size (area of more than 55 dBZ within the detected cell).

Additionally, a cell Category (0, 1 or 2) is defined based on the cell core size: Category 1 for cells with at least 1 $km^2 \geq 55$ dBZ, Category 2 for cells with at least 12 $km^2 \geq 55$ dBZ (Category 2a) or at least 1 $km^2 \geq 60$ dBZ (Category 2b) and Category 0 for all other cells. Mason (1971) first suggested a threshold of 55 dBZ for the assessment of hail.

Forecasters at the German Weather Service (DWD, Deutscher Wetterdienst) and emergency managers use KONRAD operationally. Furthermore, it is used as input for automated warning guidance (James et al., 2018). Wapler (2017) analysed KONRAD cell attributes for several hundred observed hailstorms. Some verification results for KONRAD are given in Wapler et al. (2012). The relation of some cell attributes to the prevailing synoptic pattern is described in Wapler and James (2015).

2.2. Mesocyclone detection

The distinction between non-mesocyclonic and mesocyclonic storms in this study is based on the mesocyclone detection algorithm (MCD) implemented at DWD. It utilises 3D Doppler radar data measured at 10 elevations (0.5° to 25°) at the 17 operational radar sites. A quality control algorithm is applied to this data in order to filter out dual-PRF unfolding errors, which could induce false values of azimuthal shear.

The identification of the high shear region in the centre of mesocyclonic rotation can be achieved using a pattern vector approach. It finds the velocity couplet in the radial wind data from the individual scans at all elevations and radar sites. These detected two-dimensional features are then grouped to three-dimensional mesocyclone objects. A number of properties from the categories geographical coordinates, shape, Doppler velocity, and reflectivity attributes are provided for each detected mesocyclone. Based on the geometry and the strength of the rotation the mesocyclones are classified into 5 severity levels, implying mesocyclonic rotation with increasing confidence and strength. To be classified as a mesocyclone with a certain severity level, the mesocyclone equivalent diameter and the mesocyclone depth have to exceed certain thresholds. The diameter has to be above 3 km for severity levels 1 and 2, and above 5 km for severity levels 3, 4, and 5. The depth has to reach 1 km for severity level 1, 2 km for level 2, 3 km for level 3, 6 km for level 4, and 8 km for level 5. Additionally, either the maximum azimuthal shear or the maximum rotational velocity has to exceed the following thresholds: azimuthal shear above 5, 7, 10, 20 and $30 \cdot 10^{-3}\ s^{-1}$, and rotational velocity above 36, 43.2, 54, 72 and 90 km/h (i.e. 10, 12, 15, 20 and 25 m/s) for severity levels 1, 2, 3, 4 and 5, respectively.

A detailed description of the algorithm along with some illustrative case studies and a statistical analysis is given in (Hengstebeck et al., 2018). Further statistical analyses of mesocyclone characteristics can also be found in Wapler et al. (2016). Detected mesocyclones every 5 min are available since 2013.

2.3. Lightning stroke data

The European VLF/LF LIghtning detection NETwork (LINET, Betz et al., 2009) measures lightning strokes using the time-of-arrival (TOA) method. It measures both intra-cloud/inner-cloud (IC) as well as cloud-to-ground (CG) strokes. Data is provided with a quasi continuous temporal and spatial resolution. The data have an average statistical spatial accuracy of approximately 150 m and comparable detection efficiency as other lightning location systems operating in the VHF and VLF/LF range according to Betz et al. (2009). It is assumed that the detection efficiency is adequately even within the analysis domain.

For each measured stroke, the location (latitude/longitude) and time is given along with some attributes. The strokes are not grouped to flashes. Total lightning TL (i.e. all strokes (IC and CG)) is used.

The lightning stroke data is used to support operational warning and forecasting at DWD since mid 2006 and also as input for nowcasting applications (James et al., 2018). A climatological analysis using these data was performed by (Wapler, 2013).

2.4. Combined data set

The combined data set consists of all detected KONRAD cells and the corresponding number of strokes for the summer seasons 2007 to 2017. The strokes which occurred within 15 km around the cell centre in a 5-min time window centred on the cell detection time are attributed to a cell. As shown by (Wapler, 2017) and reconfirmed in the current analysis, the selected distance threshold for counting strokes belonging to detected convective cells is reasonable. The associated mesocyclones detected at the same reference time were added to this data set for the summer seasons 2013 to 2017. This combined multi source data set allows studying the temporal evolution of the radar reflectivity, rotational and lightning characteristics along convective storm tracks. In the following, the term mesocyclonic storm is used for those storm tracks with at least one mesocyclone detection during the storms' lifetime. The severity of the most intense detected mesocyclone along the track determines the severity of this mesocyclonic storm track. Similarly, a storm with at least one detection along the track with

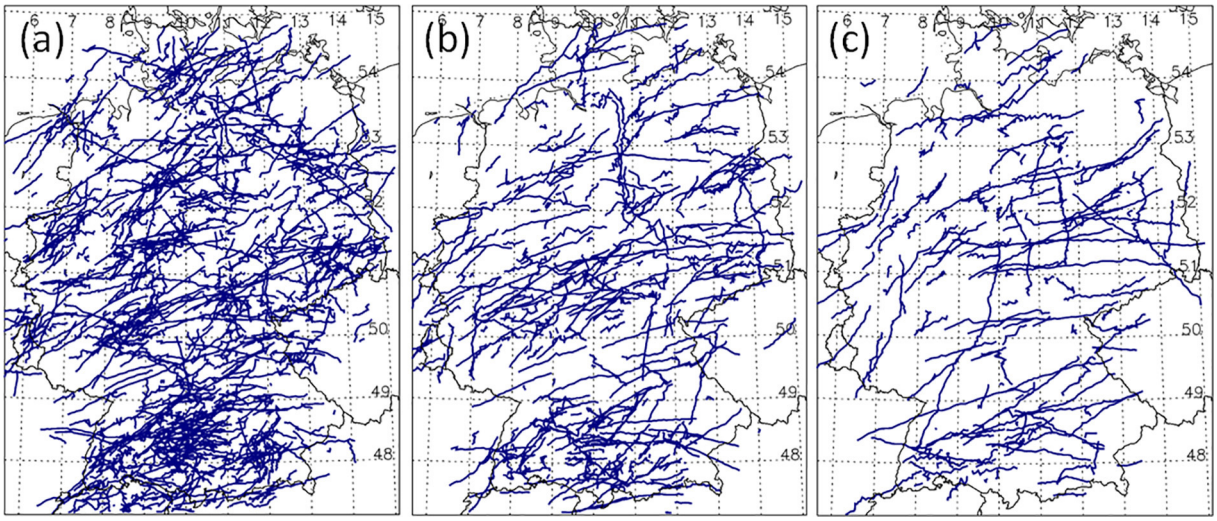

Fig. 1. Map of mesocyclonic storm tracks between April and September 2013 to 2017: (a) tracks with maximum mesocyclone severity 2, (b) tracks with maximum mesocyclone severity 3 and (c) tracks with maximum mesocyclone severity 4 and 5.

reflectivity-based cell Category 1 (2) is termed Category 1 (2) storm.

Additionally, the lightning stroke measurements and mesocyclone detections are also analysed individually.

3. Spatial and temporal occurrence

The analysed storms occurred in all parts of Germany (Fig. 1). Clearly, the frequency of storms varies from one geographical region to the other. The spatial distribution of thunderstorms in this domain is described in detail in Wapler (2013) based on a lightning climatology. The highest number of lighting strokes is recorded in the pre-alpine region with further local maxima in low mountain ranges. The analysed storms generally follow this average spatial distribution. The multi-year data set includes storms in all parts of Germany. Both short-living as well as long-living storms are observed in the whole analysis domain.

There is also no particular region prone to supercells. As shown in Fig. 1, mesocyclonic storms occur in all parts of Germany. This applies for weak and strong mesocyclones. Mesocyclonic storms generally follow the average spatial distribution of convective storms in the analysis domain.

There is a pronounced maximum of convective storm activity in this region during summer. Convective storms, non-severe and severe, are most frequent in the afternoon (Wapler, 2013, 2017). The amplitude of the diurnal cycle is largest in spring and the daily maximum occurs later in the afternoon in summer compared to spring and autumn (Wapler, 2013). The decrease of frequency in the late afternoon of non-mesocyclonic storms is faster compared to mesocyclonic storms (Wapler et al., 2016).

4. Storm attributes

First, the storm attributes are analysed. The storms movement speed and direction, radar reflectivity, lightning rate and lifetime are studied. The evolution of the storm's attributes during the convective life-cycle is discussed in *sec.* 5.

4.1. Storm lifetime

The storms' lifetime is defined as the time elapsed between the first and last detection with KONRAD. In case of only one detection the lifetime is defined as 5 min. A storm with 12 successive detections has a lifetime of 1 h.

Fig. 2 shows the lifetime of the analysed storms. The fraction of non-

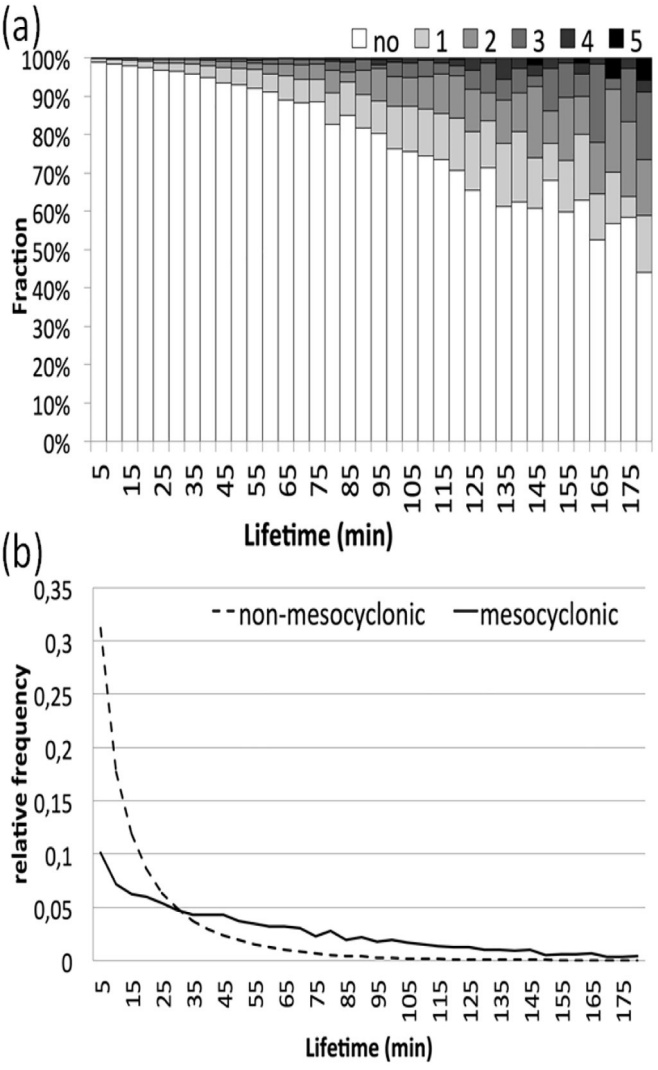

Fig. 2. (a) Fraction of non-mesocyclonic and mesocyclonic storms (severity 1, 2, 3,4 and 5) for each cell lifetime. (b) Frequency distribution of the lifetime of non-mesocyclonic and mesocyclonic storms.

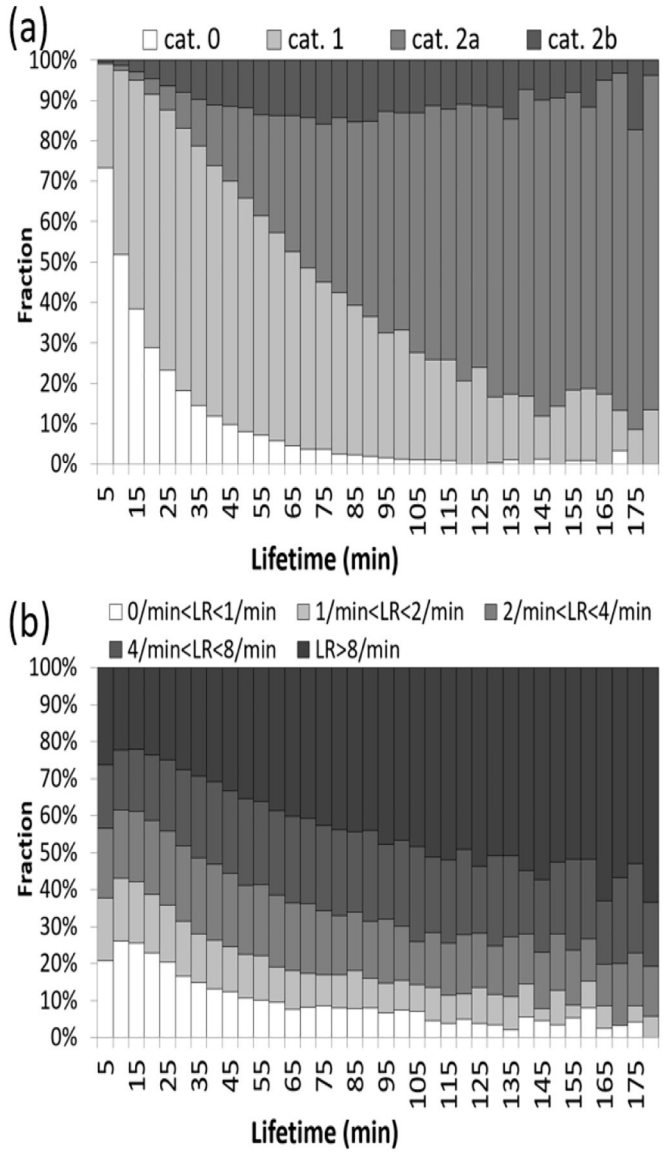

Fig. 3. Fraction of storms with different intensity for each cell lifetime: (a) reflectivity-based cell Category; (b) average lightning rate.

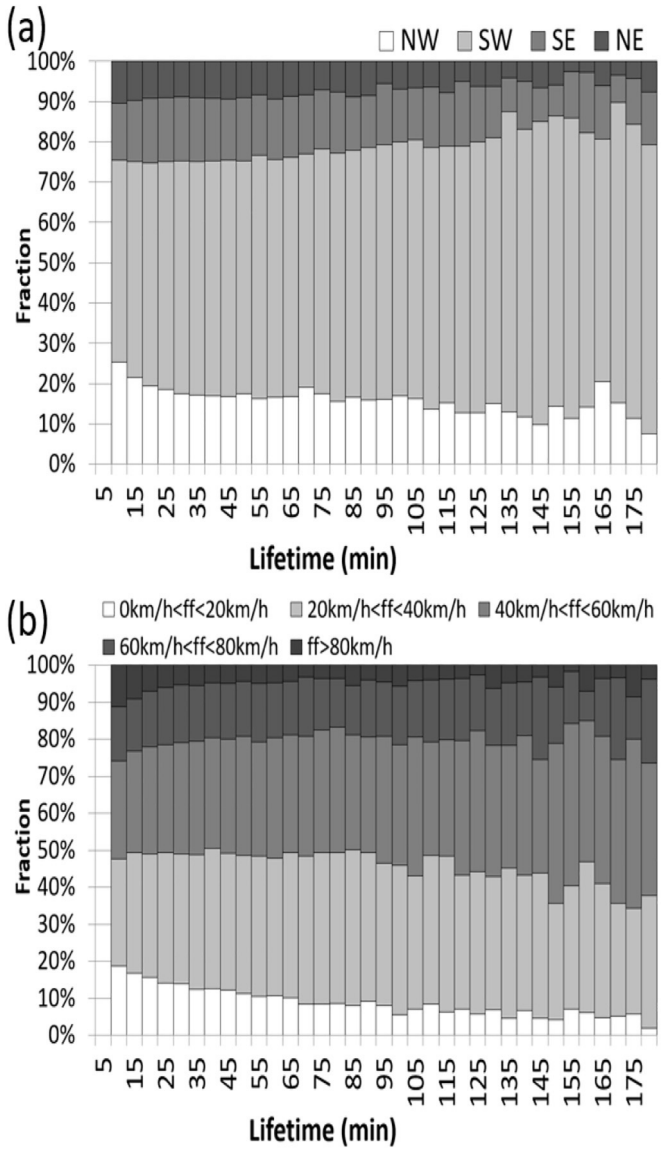

Fig. 4. Fraction of storms with different cell motion for each cell lifetime: (a) cell origin; (b) speed of cell propagation.

mesocyclonic and mesocyclonic storms for each lifetime is given in Fig. 2a. 4% of all storms with a lifetime of upto 60 min are mesocyclonic. This fraction increases with lifetime. Approximately 40% of all storms that are tracked for 2 h or more are mesocyclonic storms. The fraction of severe mesocyclones also increases with lifetime. The relative frequency of different lifetimes for non-mesocyclonic and mesocyclonic storms is shown in Fig. 2b. While it decreases rapidly for non-mesocyclonic storms, the decrease is much slower for mesocyclonic storms. Mesocyclonic storms with a lifetime of 90 min are half as frequent as those with a lifetime of 30 min, whereas non-mesocyclonic storms with a 30 min long track occur twelve times as often as those with a 90 min long track. The median lifetime of mesocyclonic storms is approx. 30 min longer than the median lifetime of non-mesocyclonic storms.

Storms, which reach Category 2, are longer living than Category 1 storms, which are longer living than Category 0 storms. Category 2b storms (at least 1 $km^2 \geq 60$ dBZ but < 12 $km^2 \geq 55$ dBZ) have shorter lifetimes compared to Category 2a storms (≥ 12 km^2 with ≥ 55 dBZ) but nevertheless longer lifetimes than Category 1 storms. The fraction of storms with the different cell Categories for each lifetime is given in Fig. 3a. The fraction of Category 0 storms decreases rapidly with increasing lifetime. Category 2a are most common for longer lifetimes. Nearly all storms with a lifetime of 120 min or longer reach either Category 1 (approx. 20%) or Category 2 (approx. 80%) whereas approx. 52% of all storms with a lifetime of upto 30 min reach this Category. The fraction of storms with higher average lightning rate also increases with increasing lifetime (Fig. 3b). 21% of all storms with a lifetime of upto 30 min have an average lightning rate of less than 1 per min, 25% of those storms have an average lighting rate of more than 8 strokes per minute. Only 4% of storms with a lifetome of 2 h or more have less than 1 stroke per minute on average, while the lightning rate of more than 50% of those storms is above 8 strokes per minute.

The lifetimes of storms with different motion are shown in Fig. 4 seperating the storms into four sectors (originating from NW, SW, SE, and NE) and into five velocity ranges (below 20 km/h, 20 to 40 km/h, 40 to 60 km/h, 60 to 80 km/h and above 80 km/h). In contrast to the clear dependence of the frequency of storms with different rotation and intensity characteristics, the lifetime is only weakly linked to the cell motion. The fraction of the storms propagating from SW to NE increases from slightly above 50% for very short living storms to appox. 75% for longer living storms (Fig. 4a). Very slow (below 20 km/h) and very fast (above 80 km/h) cell speeds are increasingly unlikely for storms with

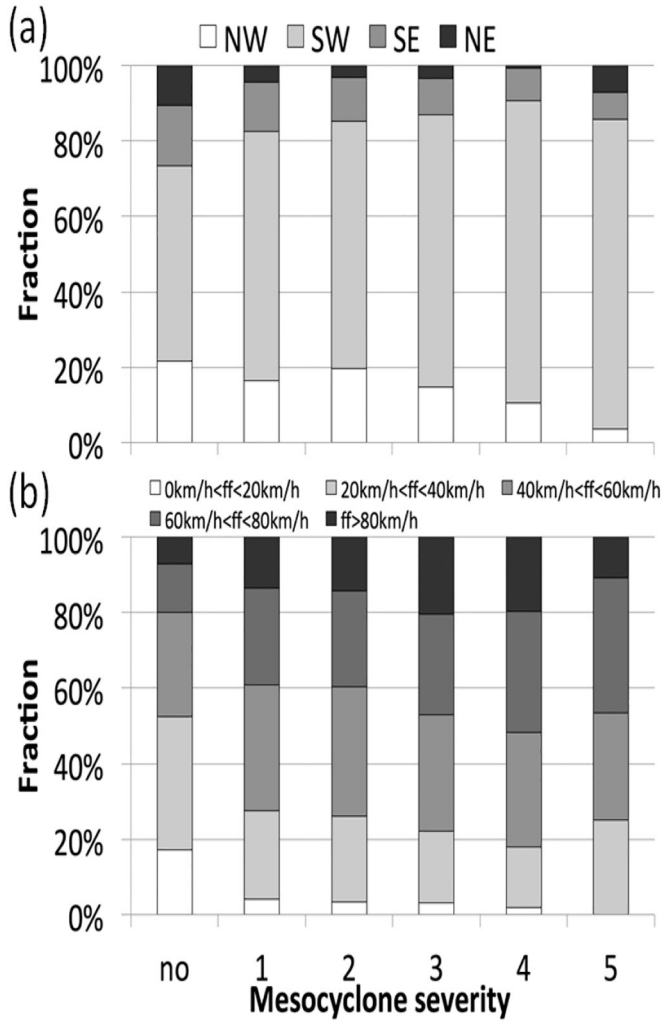

Fig. 5. Comparison of the cell motion of non-mesocyclonic and mesocyclonic storms (severity 1, 2, 3,4 and 5): (a) cell origin and (b) speed of cell propagation.

longer lifetimes (Fig. 4b).

The lifetime of convective storms might also depend on the convective organisation linked to the initiation mechanism. Using idealised cloud-resolving simulations Houston and Wilhelmson (2011) analysed the longevity of isolated storms versus quasi-linear convective systems. They showed that quasi-linear mechanisms that initiate multiple cells in close proximity can lead to longer-lived storms than mechanisms initiating isolated storms.

The statistic of storm lifetimes is influenced by the difficulties any cell tracking algorithm encounters when following individual cells with a unique ID in complex convective situation (see also Section 2.1).

4.2. Storm motion

Most of the storms propagate from SW to NE or W to E (Figs. 6b), storm motions towards all other directionare far less common with a minimum of storms moving to the South. This distribution is even more pronounced for mesocyclonic storms. The fraction of storms moving to south-eastern or south-western directions decreases with lifetme (Fig. 5a). Some of the mesocyclonic storm tracks bend to the right (Fig. 1), so called right movers. Mesocyclonic storms propagate much faster than non-mesocyclonic storms (Fig. 6a), the average speed is approx. 42 km/h (56 km/h) for non-mesocyclonic (mesocyclonic) storms. The median speed of non-mesocyclonic storms (slightly below

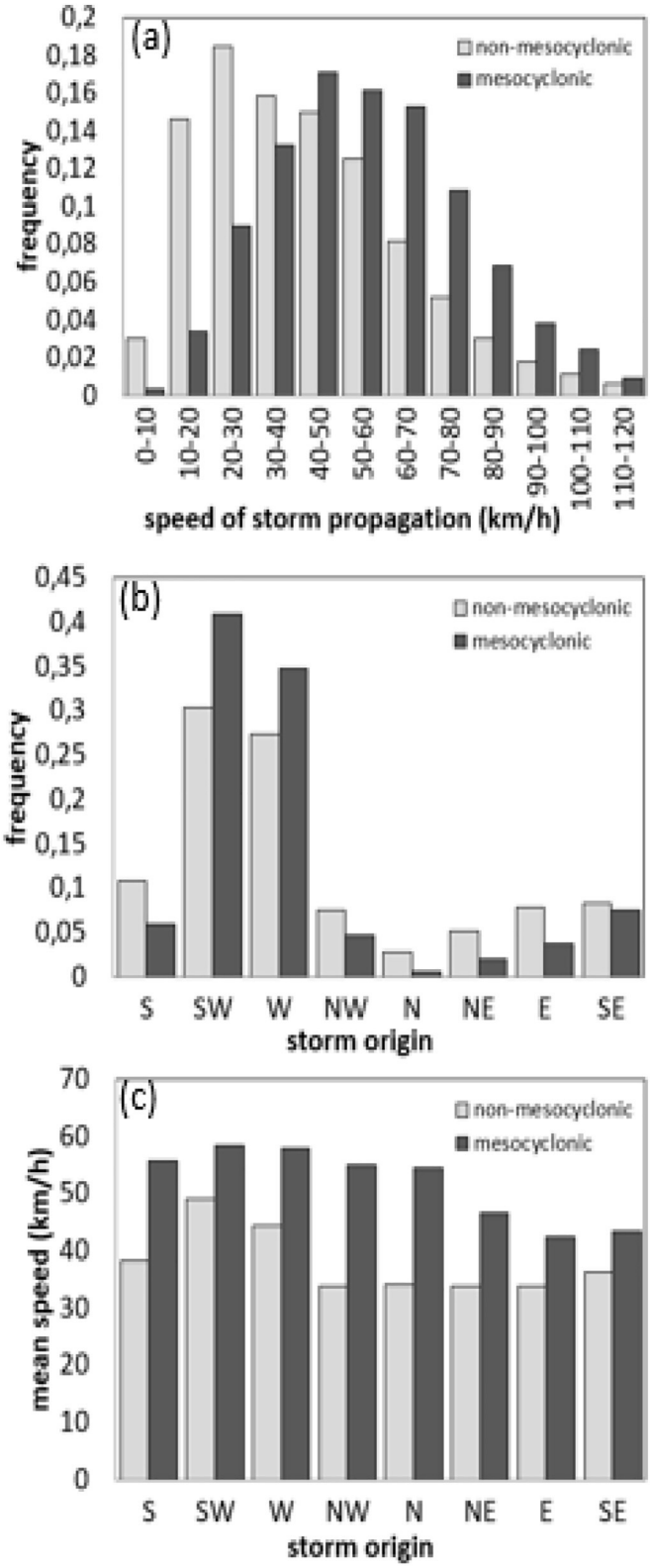

Fig. 6. Cell motion of non-mesocyclonic and mesocyclonic storms: (a) speed of storm propagation, (b) storm origin and (c) mean speed as function of storm origin.

40 km) is reached by approximately 80% of strong mesocyclonic storms. The differences in movement speed and direction increase with increasing mesocyclone severity (Fig. 5). The average movement speed varies for different storm motion directions (Fig. 6c). The speed of non-

mesocyclonic storms is highest (approx. 49 km/h) for storms originating form the SW and lowest (approx. 34 km/h) for storms originating form the NW,N,NE or E. The average speed of mesocyclonic stroms varies between 58 km/h for storm origination from the SW or W and approx. 42 km/h for storms originating form the E.

The dependence of the storm motion on the prevailing synoptic pattern is shown by Wapler and James (2015). They showed that during westerly symoptic patterns, which are associated with relatively strong winds in mid-levels, the storm motion is higher compared to other synoptic patterns. Related to the predominant synoptic flow, the average convective cell speed is faster in winter with a cell propagation in eastern and southeastern directions.

A well-known rough rule of thumb is the estimation that convective cells propagate with the wind at 700 hPa. This relationship was established by Ligda and Mayhew (1954) and further studied by Marshall (1980). While widely applied and supported for many individual cases, the relationship between cell motion and winds at so-called steering levels can be much more complicated as discussed by Carbone et al. (2002).

The propagation speed of non-mesocyclonic and mesocyclonic storms was compared to the wind speed at the 700 hPa level using data from the limited area COSMO model (consortium for small scale modelling; Baldauf et al. (2011)). In general, the cell propagation and wind speed at 700 hPa are correlated with a correlation coefficient of 0.62 for non-mesocyclonic storms, 0.55 for mesocyclonic storms and 0.51 for mesocyclonic storms with a maximum severity of or above 2. On average, storms with a propagation of 45 km/h move with the speed of the 700 hPa wind, while for faster moving storms the storm motion is faster than the 700 hPa wind and for slower moving storms the storm motion is slower than the 700 hPa wind. This is more pronounced for mesocyclonic storms than for non-mesocyclonic storms. On average the speed of the 700 hPa wind is approx. 25 km/h for non-mesocyclonic and approx. 28 km/h for mesocyclonic storms which propagate with 20 km/h. In contrast, the wind at 700 hPa is on average approx. 71 km/h for non-mesocyclonic and approx. 64 km/h for mesocyclonic storm which propagte with 80 km/h.

4.3. Storm intensity

The average lightning rate calculated over the entire lifetime of the storm (i.e. the total number of strokes divided by the storms' lifetime) is shown in Figs. 3b and 7a. The average lightning activity of mesocyclonic storms is much higher compared to non-mesocyclonic storms. The higher the mesocyclone severity the higher the average lightning rate (Fig. 7a) (e.g. 25% of non-mesocyclonic storms reach values of 8 strokes per minute, whereas 70% of weak meso-cyclonic storms (severity 1) and all of the strongest mesocyclonic storms (severity 5) reach this value).

The spatial distribution of lightning strokes around the storms centre is given in Fig. 8. The average lightning activity increase with increasing mesocyclone severity. The majority of the lightning strokes occur around the storm centre. The radius with high lightning density increases with severity. (Note that for the strongest mesocyclones only a low number of cases (188 for severity 4 and 39 cases for severity 5) occurred, thus the spatial distribution is not as smooth as for weaker mesocyclones.) The figure shows the average lightning rate per km^2 for all cell detections. For the mesocyclones the severity at the time of each detection is considered, however, the time of the maximum rotation is not necessarily the time of strongest lightning activity. Stough et al. (2017) analysed the relationship between lightning and mesocyclonic rotation in supercell thunderstorms. They found lightning jumps prior to mesocyclone intensification in the majority of analysed storms. Analysis by Wapler (2017) showed that half of the hailstorms in Germany, which were mainly associated with mesocyclonic storms, have pulsating lightning activity.

In general, the average 1-min lightning rate is higher for long-living

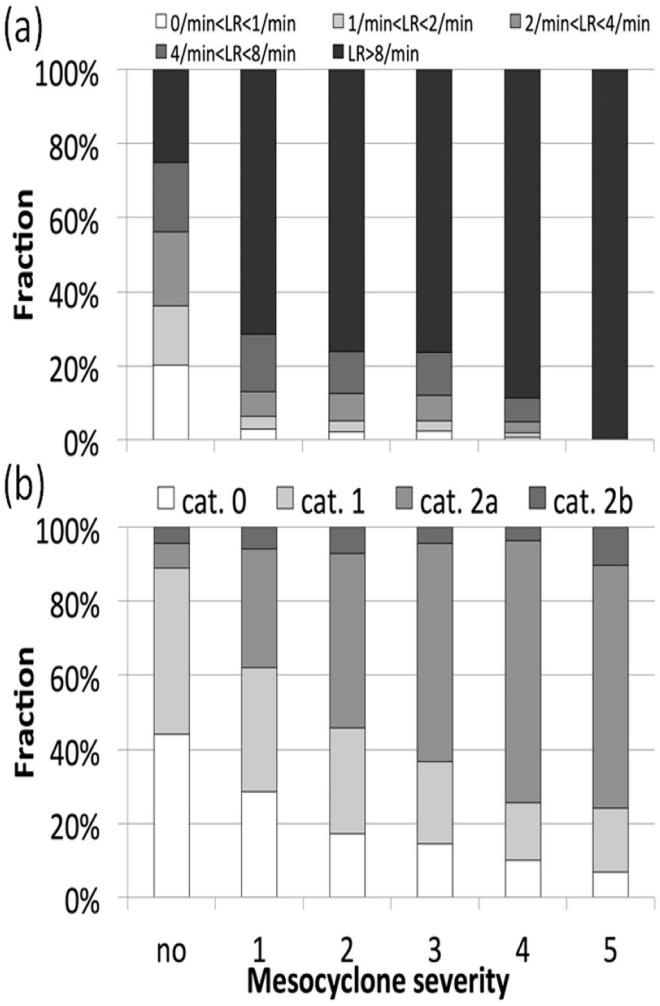

Fig. 7. Comparison of cell attributes of non-mesocyclonic and mesocyclonic storms (severity 1, 2, 3,4 and 5): (a) average lighting rate and (b) maximum cell Category (cat. 0: reflectivity below 55 dBZ, cat. 1: at least 1 km^2 ≥ 55 dBZ, cat. 2a: at least 12 km^2 ≥ 55 dBZ, cat. 2b less than 12 km^2 ≥ 55 dBZ but at least 1 km^2 ≥ 60 dBZ).

cells. However, on average even long-living non-mesocyclonic storms have weaker lightning activity compared to mesocyclonic storms. In some nowcasting applications (e.g. the nowcasting algorithms / storm severity classifications used by the German Weather Service (James et al., 2018), the Finish Meteorological Service (Rossi et al., 2014) and the National Weather Service of the U.S. (Cintineo et al., 2018)) the lightning density is used as descriptor in conjunction with radar reflectivity based parameters to estimate the probability of hail. Wapler (2017) showed that the local lightning density of the hail events with larger observed hail diameter is higher than the lightning density of hail events with smaller hail diameter.

Wapler (2017) introduced a lightning jump intensity which describes the strength of the lightning jump depending on the strength of the rapid increase in the lightning rate as well as the resulting lightning rate. The lightning jump intensity increases from 0 (for values of the strength of the rapid increase as well as the lightning rate just above 0) to 1 (for the highest values of those parameters), a lightning jump intensity of 0.2 is comparable to the original lightning jump definition by (Schultz et al., 2009) who used fixed thresholds. Using this lightning jump calculation, approximately 20% of the short-living and 66% of the long-living storms of Category 2 have a lightning jump with intensity 0.2. For a strong lightning jump with intensity 0.5, the fraction of Category 2 storms with lightning jump is approximately 7% for short-

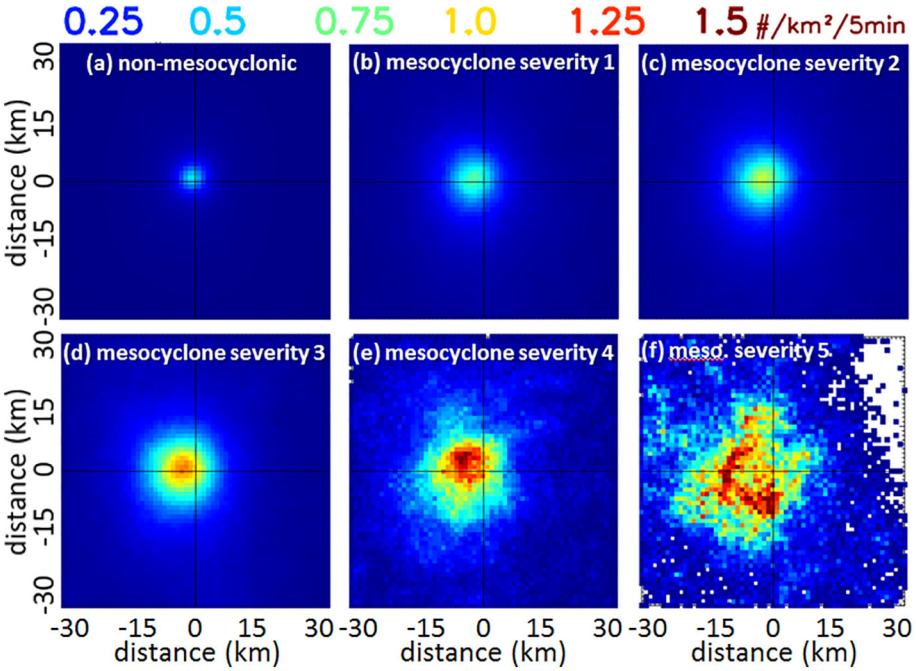

Fig. 8. Local mean lightning density (in 1/km^2/5 min) for (a) all detected KONRAD cells with at least one stroke within 15 km, (b-f) all detected mesocyclones with severity 1, 2, 3, 4 and 5, respectively. The analysis is based on data from April to September 2013 to 2017. The cell centre is in the plot centre.

living and 35% for long-living storms.

Mesocyclonic storms have higher reflectivity (Fig. 7b). While approximately 45% of non-mesocyclonic storms don't reach reflectivity ≥ 55 dBZ, three quarters of mesocyclonic storms have maximum reflectivity with ≥ 55 dBZ. More than 50% of the strong mesocyclones have convective cores with more than 12 km^2 with reflectivity ≥ 55 dBZ.

Storms with Category 1 and 2 are more frequent in the afternoon compared to the rest of the day (not shown). They are also more frequent in summer.

5. Storm life-cycle

The life-cycle (i.e. the temporal evolution of storm attributes throughout the storms lifetime) is analysed in the following. For each lifetime, the life-cycle is analysed separately. For this purpose, the storms are grouped according to their lifetime. According to the frequency distribution of storm lifetimes, the sample size for longer lifetimes is much smaller compared to shorter-living storms (e.g. more than 8000 storms with a lifetime of 25 min and slightly more than 300 storms with a lifetime of 100 min for the summer seasons (April to September) 2007–2017). During the 5-year period from 2013 to 2017, 3580 non-mesocyclonic and 147 mesocyclonic storms had a lifetime of 25 min; 131 non-mesocyclonic and 46 mesocyclonic storms had a lifetime of 100 min. Thus, the curves are smoother for shorter lifetimes. The temporal evolution of storm attributes varies from one storm to the other, however, general tendencies become visible.

5.1. Temporal evolution of storm attributes

This analysis is based on data from 2007 to 2017, however, the results are qualitatively similar when using data from 2013 to 2017.

The temporal evolution of the cell size (area with reflectivity ≥ 46 dBZ) from its first to its last detection is shown in Fig. 9a. The median is shown for each lifetime. As expected, on average the cell size increases during the first half of the lifetime, reaches its maximum and decreases afterwards. Linked to the cell detection criterion the initial cell size is similar for all lifetimes. The growth rate is comparable for all lifetimes. The average maximum cell size increases with storm longevity. The median cell size along with the 25th- and 75th-percentile is given in Fig. 9b for the four selected lifetimes 25 min, 50 min, 75 min and 100 min. This shows the variability of the temporal evolution of the cell size of the storms within the analysed sample. The interquartile range (IQR) is smallest at the beginning and at the end of the lifetime and largest during the time of the maximum. The IQR also increases with the increasing maximum for longer lifetimes. The IQR is 9 km^2 at the beginning independent of the storm lifetime and 17 km^2 (48 km^2) during the time of the maixumum for storms with a lifetime of 25 min (75 min).

For individual cells, the cell size might not grow continuously until it reaches its maximum and also might not decay continuously afterwards, but may fluctuate. Thus, the cell size tendency (i.e. the difference of the cell size from one time step to the next) is also variable.

Fig. 9c shows the temporal evolution of the cell core size (area with reflectivity ≥ 55 dBZ). Due to the spatial resolution of the radar reflectivity measurements, only discrete values of km^2 are possible for the cell area and cell core area, thus, the cell core areas shown in the figure show a stepped distribution. While the 25th-percentile equals 0 throughout the lifetime of shorter and longer living storms, the maxima of the median (75th-percentile) increases with storm longevity, from 1 (5) for storms with a lifetime of 50 min to 4 (12) for storms with a lifetime of 100 min. Similar to the cell size, on average the maximum of the cell core size is reached at the middle of the storms lifetime. However, this may be different for individual storms. Relating the cell core size to the cell size for the different lifetimes show that the cell core fraction (i.e. the fraction of the cell with reflectivity ≥ 55 dBZ) reaches higher values for longer-living storms (not shown).

The temporal evolution of the median lightning rate is shown in Fig. 9d. It first increases, reaches its maximum after the middle of the lifetime and decreases afterwards. However, at the end of the lifetime it is higher that the initial median at the time of the first detection. This is due to the definition of lifetime in this study, which is defined as the time a storm is detected in radar reflectivity data using certain thresholds. Many storms still produce lightning strokes while the storms refelctivity and size drop below the detection criterion. In contrast, the lightning activity at the begining (with the same reflectivity and size

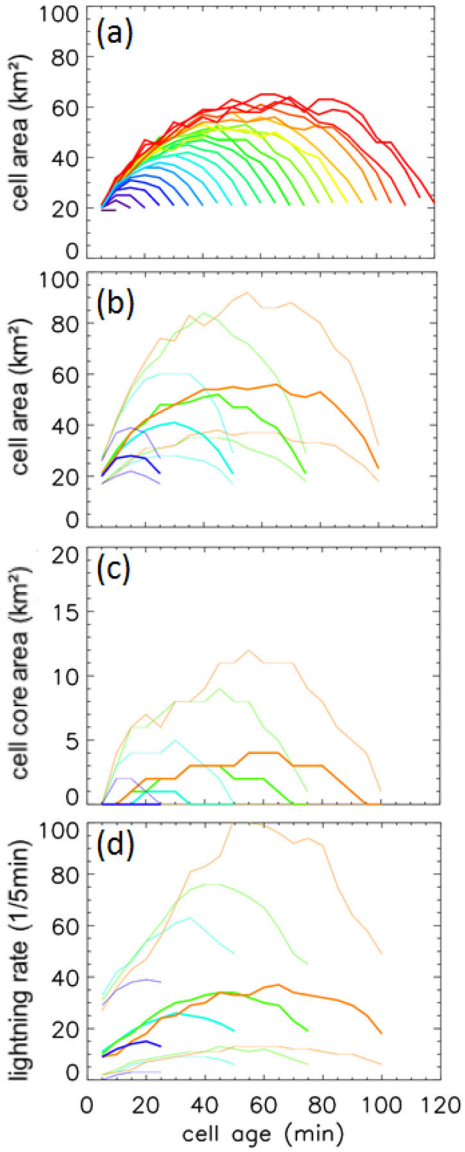

Fig. 9. Temporal evolution of cell attributes as function of the lifetime. (a) Median cell area (area with at least 46 dBZ) of all cells with a lifetime of 10, 15, 20, 25.0.120 min (from blue through green and yellow to red). (b) 25th-percentile (thin), median (thick) and 75th-percentile (thin) of cell area for all cells with a lifetime of 25 min (8628 cells; blue lines), 50 min (2194 cells; cyan lines), 75 min (774 cells; green lines) and 100 min (312 cells; orange lines). (c) Same as (b) but for cell core are (area with at least 55 dBZ). (d) Same as (b) but for 5-min lightning rate (number of strokes within 15 km). The analysis is based on data from April to September 2007 to 2017.

thresholds) is lower. The IQR is largest during the time of the maximum. Throughout the lifetime, the IQR of the lightning rate is much larger than the IQR of the cell size (e.g. maximum IQR of 54 with a median lightning rate of 25 per 5 min for storms with 50 min lifetime compared to a IQR of 32 with a median cell area of 40 km^2 for those storms). This is due to a larger variability of the lightning activity during the storms life-cycle (e.g. caused by pulsating lightning rates or lightning jumps). Furthermore, the increase of the IQR with longer lifetimes is much more pronounced compared to the cell size. Lightning jumps or pulsating lightning activity, which are induced by a re-intensification of the storms updraft (Dotzek et al., 2005; DiGangi et al., 2016), are more frequent for longer living storms. The relation of storm longevity to the occurrence and intensity of lightning jumps was also shown by Chronis et al. (2015).

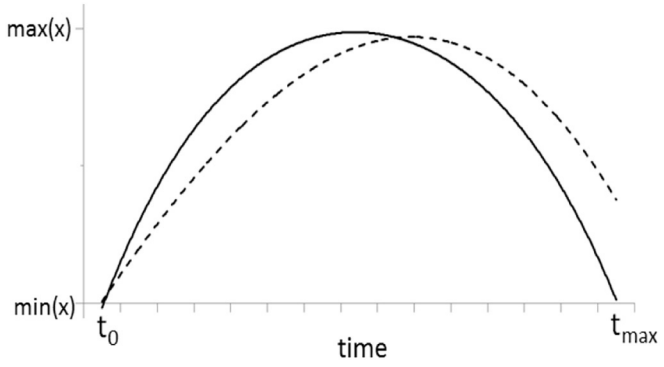

Fig. 10. Schematic of the temporal evolution of the median cell size (area with at least 46 dBZ; solid) and median 5-min lightning rate (number of strokes within 15 km; dashed) as function of the lifetime for all cells with a lifetime of 75 min. Both parameters are scaled to its value at the time of the first detection and the maximum. The analysis is based on data from April to September 2007 to 2017.

The smoothed temporal evolution of the median cell size and the median 5-min lightning rate as function of the lifetime is depicted in Fig. 10. Both parameters are scaled to their value at the beginning of the storms life-cycle and during time of the maximum. It illustrates the different temporal evolution: while the increase and decrease of the cell size is symmetric to the time of the maximum, which lies in the middle of the lifetime, the lightning rate increases slower, reaches its maximum later and does not drop to the initial value. Fig. 10 is derived from the storms with a lifetime of 75 min, however, it looks qualitatively similar for other lifetimes. The time between the average temporal evolutions of cell size and lightning rate is approx. 10 min for storms with a lifetime of 75 min.

5.2. Life-cycle depending on storm attributes

Using data from the summer seasons 2013 to 2017, the difference between the life-cycle of non-mesocyclonic and mesocyclonic storms is analysed. The distinction of mesocyclonic storms with different severity is not possible for the life-cycle analysis due to the limited sample size for individual lifetimes.

Mesocyclonic rotation is not detected during all times in the storms lifetime. Each storm starts as small single cell before forming an intense rotating updraft. The convective cell will intensify with increasing lifetime, and in case of a supercell develop a mesocyclone. During the most intense phase of the storm, the rotation and size usually maintains and then weakens subsequently, represented by the mesocyclone severity levels. Detailed case studies of such temoporal evolutions are discussed in Hengstebeck et al. (2018) and Wapler et al. (2016). Additionally, Hengstebeck et al. (2018) showed that the mesocyclone fraction (i.e. the fraction of the KONRAD lifetime where mesocyclone detections could be associated) is between 0.1 and 0.5 for 70% of the mesocyclonic storms. The average time between successive mesocyclone detections along the storm track is 5 or 10 min for approximately 85% of all mesocyclonic storms (with 5 min as smallest possible time difference according to the radar scan interval).

The temporal evolution of the cell size is shown in Fig. 11. Related to the cell definition and thus the detection criterion, the initial cell size is similar for non-mesocyclonic and mesocyclonic storms for all lifetimes. The median cell size increases faster for mesocyclonic cells. When comparing Fig. 11 and Fig. 9, it can be seen that the median cell size of mesocyclonic storms (Fig. 9) is comparable to the 75th-percentile of non-mesocyclonic storms (upper thin line in Fig. 9) (e.g. the median cell size of mesocyclonic cells with a lifetime of 25 min reaches a maximum of approx. 40 km^2 similar to the 75th-percentile of non-mesocylonic storms with the same lifetime). Despite differences in the

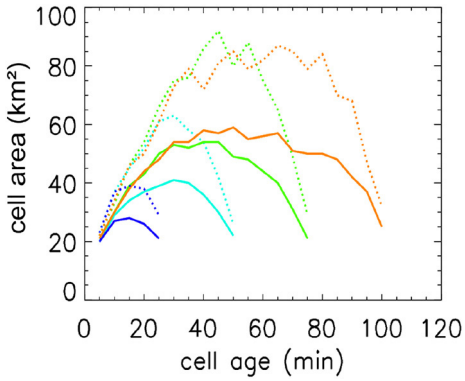

Fig. 11. Temporal evolution of the median cell size (area with at least 46 dBZ) for non-mesocyclonic cells (solid) and mesocyclonic cells (dotted) with a lifetime of 25 min (3580 / 147 cells; blue lines), 50 min (907 / 104 cells; cyan lines), 75 min (328 / 51 cells; green lines) and 100 min (131 / 46 cells; orange lines). The cell numbers refer to non-mesocyclonic/mesocyclonic cells. The analysis is based on data from April to September 2013 to 2017.

beginning, the relative trend of the cell size of mesocyclonic storms is comparable to and within the IQR of the relative trend of non-mesocyclonic cell sizes. The median cell core sizes of mesocyclonic storms are higher compared to the median of non-mesocyclonic storms, however, clearly within the IQR.

The lightning rate is more variable in mesocyclonic storms. Especially, pulsating lightning activity and lightning jumps are more frequent in those storms (Stough et al., 2017; Wapler, 2017). As an example, a mesocyclonic storm with a lifetime of 100 min is chosen: the maximum lightning rate was 260 strokes per 5 min, followd by a secondary maximum of 135 per 5 min 40 min later; the lightning rate steadily dropped to 57 strokes in between these two maxima. This storm produced hail and is illustrated in Wapler (2017). The median lightning rate of mesocyclonic storms is above the 75th-percentile of non-mesocyclonic storms throughout the life-cycle of storms with short and median lifetimes. It is slightly below the 75th-percentile only for storms with lifetimes of 100 min, however, this might be due to the smaller sample size.

Storms with no lightning stroke at the time of their first detection have smaller maximum of the median cell size (e.g. approx. 80% compared to the sizes of storms with strokes at the time of first detection; Fig. 12a), smaller median core sizes, and thus reach cell Category 1 and 2 less often. Furthermore, they have smaller median lightning rates throughout the life-cycle (Fig. 12b); the median reaches 30% and the difference between intital lightning rate and maximal medain lightning rate reaches 50% compared to storms with lightning strokes allready at the time of their first detection. When comparing Fig. 12b to Fig. 9d, it can be seen that the median lightning rates of storms without strokes at the time of their first detection (Fig. 12b) are similar to the 25th-percentile of the lightning rates of all other storms (Fig. 9d).

As expected, storms of Category 2 also have higher median cell sizes and lightning rates throughout their lifetime compared to Category 1 and 0. However, they do not reach the median values of mesocyclonic storms, especially in terms of lightning activity.

When grouping the storms according to their direction and speed, the sample sizes are small especially for less common movements to the South-West and less common long-living stationary storms. In general, the differences in the life-cycle of storms propagating in different directions and with different speed are only small; the median of cell attributes of the different groups are well within the IQR of the other groups. Cell sizes are similar at the beginning and end of the lifetime. Storms propagating to the South-East have smaller median cell sizes (sizes of approximately 88% relative to the size of all storms) in the middle of the lifetime of short and medium lifetimes. The median cell size is smaller (sizes of approximately 85% relative to the sizes of all

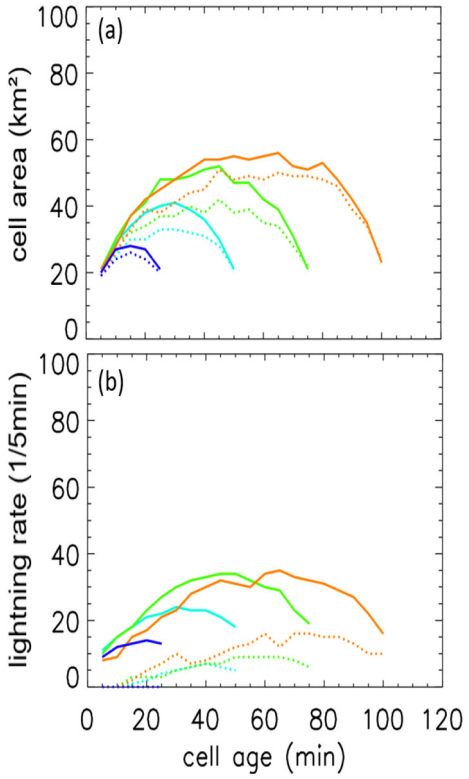

Fig. 12. Temporal evolution of median cell attributes for all cells (solid) and cells with no lightning strokes at the time of the first cell detection (dotted) with a lifetime of 25 min (blues lines), 50 min (cyan lines), 75 min (greean lines) and 100 min (orange lines): (a) median cell size (area with at least 46dBZ); (b) 5-min lightning rate (number of strokes within 15 km). The analysis is based on data from April to September 2007 to 2017.

storms) for stationary and slow moving ($\leq$ 20 km/h) and larger (sizes of approximately 110% relative to the sizes of all storms) for fast moving ($\geq$ 60 km/h) storms. However, the median cell core fraction is largest for slow moving and smaller for fast moving storms. The median lightning rates are smaller (lightning rates of approximately 80% relative to all storms) for storms moving to the South-East and larger (lightning rates of approximtately 130% relative to all storms) for storms moving to the North-West throughout their lifetime.

6. Summary and conclusion

Non-mesocyclonic (more than 100,000) and mesocyclonic storms (approximately 4300) of the summer seasons (April to September) 2013 to 2017 are analysed. Those parts of the analyses which do not distinguish between non-mesocyclonic and mesocyclonic storms are based on data from the summer seasons 2007 to 2017 to have a time period as long as possible. These time periods are limited by the availability of the different data sets. Nevertheless, the analyses showed that the results are qualitatively similar for non-mesocyclonic storms of the periods 2007–2017 and 2013–2017.

The analysed multi-source data set includes measurements from a lightning location system and precipitation radar network. Non-mesocyclonic and mesocyclonic storms are identified using automated cell detection algorithms based on radar reflectivity and radial winds. The storm's rotation characteristics are analysed in conjunction with the storms reflectivity and lightning attributes as well as storm motion for different lifetimes. For this purpose, the lifetime is defined as the time a storm is automatically detected and tracked in radar reflectivity data using certain thresholds suited for deep convection, the time between the initial cloud formation and the final dissipation would be longer.

While the development of storms varies from one storm to the other, analysing the temporal evolution of various storm attributes for different lifetimes reveals typical storm developments.

The results include the following:

- On average, mesocyclonic storms have higher lightning rates, higher reflectivity and larger storm sizes than non-mesocyclonic storms.
- Mesocyclonic storms have longer lifetimes (the median is approximately 30 min longer).
- Mesocyclonic storms propagate faster (on average approximately 15 km/h faster) and more often from South-West to North-East.
- Most of the aforementioned features are more pronounced for stronger mesocyclonic storms compared to weak mesocyclonic storms.
- Storms originating from the SW propagate fastest (on average approximately 15 km/h faster than storms originating from the E).
- The speed of the 700 hPa wind is similar to that of the storm motion for storms with average propagation speed. For faster (slower) moving storms the storm motion is faster (slower) than the 700 hPa wind.
- Longer living storms reach higher reflectivity and have stronger average lightning activity.
- The lightning strokes are concentrated around the cell centre.
- The temporal evolution of the storm size is symmetric, the median cell size increases until half of the lifetime and decreases afterwards.
- The maximum lightning rate is reached later that the maximum storm size and the lightning rate does not drop to the value at the beginning of the lifetime.
- Storms with no lightning during the first detection have weaker lightning activity throughout the storms' lifetime and are smaller.
- Mesocyclonic storms grow faster compared to non-mesocyclonic storms with similar lifetimes.

The knowledge of the convective life-cycle provides valuable information for nowcasting purposes. While current nowcasting systems are mainly advection-based without a forecast of the convective evolution, such multi-year statistics of the lifetime and the temporal evolution of storm attributes can be used in the future to predict the strengthening and weakening of convective storms. E.g. a parabola opening down can be applied to describe the temporal evolution of the storm size and be used to estimate the remaining storm size evolution and with it the remaining storm lifetime. Additionally, the variability of the storms' life-cycle can be utilised to estimate the uncertainty in probabilistic nowcasting applications. Feger et al. (2019) show first approaches to consider this life-cycle information for the estimation of further cell development in a new 3D cell detection, tracking and nowcasting ensemble. Furthermore, when knowing typical characteristics of non-mesocyclonic and mesocyclonic storms derived storm multi-year data sets the automatic detection of mesocyclonic rotation - in combination with other measurements - can support forecasters in warning operations as well as nowcasting algorithms.

Author statement

All work presented in this manuscript was done by the author. There are no co-authors.

Declaration of Competing Interest

The authors declare that they have no known competing financial interests or personal relationships that could have appeared to influence the work reported in this paper.

References

Baldauf, M., Seifert, A., Foerstner, J., Majewski, D., Raschendorfer, M., Reinhart, T., 2011. Operational convective-scale numerical weather prediction with the COSMO model: description and sensitivities. Mon. Wea. Rev. 139, 3887–3905.

Betz, H., Schmidt, K., Laroche, P., Blanchet, P., Oettinger, W., Defer, E., Dziewit, Z., Konarski, J., 2009. LINET - an international lightning detection network in Europe. Atmos. Res. 91, 564–573.

Blair, S.F., Laflin, J.M., Cavanaugh, D.E., Sanders, K.J., Currens, S.R., Pullin, J.I., Cooper, D.T., Deroche, D.R., Leighton, J.W., Fritchie, R.V., Mezeul II, M.J., Goudeau, B.T., Kreller, S.J., Bosco, J.J., Kelly, C.M., Mallinson, H.M., 2017. High-resolution hail observations: Implications for nws warning operations. Wea. Forecasting 32, 1101–1119. https://doi.org/10.1175/WAF-D-16-0203.1.

Carbone, R., Tuttle, J., Ahijevych, D., Trier, S., 2002. Inferences of predictability associated with warm season precipitation episodes. J. Atmos. Sci. 59, 2033–2056.

Chronis, T., Carey, L.D., Schultz, C.J., Schultz, E.V., Calhoun, K.M., Goodman, S.J., 2015. Exploring lightning jump characteristics. Wea. Forecasting 30, 23–37.

Cintineo, J., Pavolonis, M., Sieglaff, J., Lindsey, D., Crone, L., Gerth, J., Rodenkirch, B., Brunner, J., Gravelle, C., 2018. The NOAA/CIMSS ProbSevere Model: Incorporation of Total Lightning and Validation. Wea. Forecasting 33, 331–345.

DiGangi, E.A., MacGorman, D.R., Ziegler, C., Betten, D., Biggerstaff, M., Bowlan, M., Potvin, C.K., 2016. An overview of the 29 May 2012 Kingfisher supercell during DC3. J. Geophys. Res. 121, 14316–14343. https://doi.org/10.1002/2016JD025690.

Dotzek, N., Rabin, R.M., Carey, L.D., MacGorman, D.R., McCormick, T.L., Demetriades, N.W., Murphy, M.J., Holle, R.L., 2005. Lightning activity related to satellite and radar observations of a mesoscale convective system over Texas on 7-8 April 2002. Atmos. Res. 76, 127–166.

Duda, J., Gallus, W., 2010. Spring and summer midwestern severe weather reports in supercells compared to other morphologies. Wea. Forecasting 25, 190–206.

Feger, R., Werner, M., Posada, R., Wapler, K., Blahak, U., 2019. Generation of an Object-Based Nowcasting Ensemble, 3rd European Nowcasting Conference, 24–26 April 2019, Madrid, Spain. Available at. https://www.eumetnet.eu/european-nowcasting-conference-enc-2019/.

Hengstebeck, T., Wapler, K., Heizenreder, D., Joe, P., 2018. Radar network-based detection of mesocyclones at the German Weather Service. J. Atmos. and Ocean. Technol. 35, 299–321. https://doi.org/10.1175/JTECH-D-16-0230.1.

Houston, A.L., Wilhelmson, R.B., 2011. The dependence of storm longevity on the pattern of deep convection initiation in a low-shear environment. Mon. Wea. Rev. 139, 3125–3138.

James, P., Reichert, B., Heizenreder, D., 2018. NowCastMIX: automatic integrated warnings for severe convection on nowcasting time scales at the German Weather Service. waf. https://doi.org/10.1175/WAF-D-18-0038.1.

Lang, P., 2001. Cell tracking and warning indicators derived from operational radar products. In: 30th Int. Conf. Radar Met., Munich, Germany, pp. 245–247.

Ligda, M.G.H., Mayhew, W.A., 1954. On the relationship between the velocities of small precipitation areas and geostrophic winds. J. Meteor. 11, 421–423.

Mammen, T., Lange, B., Frech, M., Desler, K., 2010. 3rd Generation of Systems in the DWD Weather Radar Network, 6th European Conference on Radar in Meteorology and Hydrology. pp. 6–10. September 2010, Sibiu, Romania. Available at. http://www.erad2010.org/pdf/POSTER/02_Advances/04_ERAD2010_0217_s.pdf.

Marshall, R., 1980. The estimation and distribution of storm movement and storm structure, using a correlation analysis technique and rain-gauge data. J. Hydrol. 48, 19–39.

Mason, B., 1971. The Physics of Clouds, 2nd edn. Clarendon Press, Oxford, Oxford monographs on meteorology.

Rossi, P.J., Hasu, V., Koistinen, J., Moisseev, D., Mäkelä, A., Saltikoff, E., 2014. Analysis of a statistically initialized fuzzy logic scheme for classifying the severity of convective storms in Finland. Meteorol. Appl. 21, 656–674.

Schmid, F., Banon Peregrin, L., Agerstern, S., Atencia, A., de Coning, E., Kann, A., Wang, Y., Wapler, K., 2019. Conference Report: third European Nowcasting Conference. Met. Zeitschrift 28, 447–450. https://doi.org/10.1127/metz/2019/0983.

Schultz, C., Petersen, W., Carey, L., 2009. Preliminary development and evaluation of lightning jump algorithms for the real-time detection of severe weather. J. Appl. Meteor. Climatol. 48, 2543–2563.

Stough, S., Carey, L., Schultz, C., Bitzer, P., 2017. Investigating the relationship between lightning and mesocyclone rotation in supercell thunderstorms. Wea. Forecasting 32, 2237–2259. https://doi.org/10.1175/WAF-D-17-0025.1.

Tuovinen, J.P., Rauhala, J., Schultz, D., 2015. Significant hail producing storms in Finland: Convective-storm environment and mode. Wea. Forecasting 30, 1064–1076. https://doi.org/10.1175/WAF-D-14-00159.1.

Wapler, K., 2013. High-resolution climatology of lightning characteristics within Central Europe. Meteor. and Atmos. Physics 122, 175–184. https://doi.org/10.1007/s00703-013-0285-1.

Wapler, K., 2017. The life-cycle of hailstorms: lightning, radar reflectivity and rotation characteristics. Atmos. Res. 193, 60–72. https://doi.org/10.1016/j.atmosres/2017.04.009.

Wapler, K., James, P., 2015. Thunderstorm occurrence and characteristics in Central Europe under different synoptic conditions. Atmos. Res. 158-159, 231–244. https://doi.org/10.1016/j.atmosres.2014.07.011.

Wapler, K., Göber, M., Trepte, S., 2012. Comparative verification of different nowcasting systems to support optimisation of thunderstorm warnings. Adv. Sci. Res. 8, 121–127. https://doi.org/10.5194/asr-1-1-2012.

Wapler, K., Hengstebeck, T., Groenemeijer, P., 2016. Mesocyclones in Central Europe as seen by radar. Atmos. Res. 168, 112–120. https://doi.org/10.1016/j.atmosres/2015.08.023.

Wapler, K., Banon Peregrin, L., Buzzi, M., Heizenreder, D., Kann, A., Meirold-Mautner, I., Simon, A., Wang, Y., 2018. Conference Report 2nd European Nowcasting Conference. Met. Zeitschrift 27, 81–84. https://doi.org/10.1127/metz/2017/0870.

Werner, M., 2017. KONRAD3D: A New Tool for Detetion and Nowcasting of Convective Cells at DWD. 2nd Europ. Nowc. Conf., Offenbach, Germany.